nature materials

ARTICLES

https://doi.org/10.1038/s41563-018-0022-8

Corrected: Publisher Correction

Universal strategy for Ohmic hole injection into organic semiconductors with high ionization energies

Naresh B. Kotadiya[1], Hao Lu[1], Anirban Mondal[1], Yutaka Ie[1,2], Denis Andrienko[1], Paul W. M. Blom[1] and Gert-Jan A. H. Wetzelaer[1]*

Barrier-free (Ohmic) contacts are a key requirement for efficient organic optoelectronic devices, such as organic light-emitting diodes, solar cells, and field-effect transistors. Here, we propose a simple and robust way of forming an Ohmic hole contact on organic semiconductors with a high ionization energy (IE). The injected hole current from high-work-function metal-oxide electrodes is improved by more than an order of magnitude by using an interlayer for which the sole requirement is that it has a higher IE than the organic semiconductor. Insertion of the interlayer results in electrostatic decoupling of the electrode from the semiconductor and realignment of the Fermi level with the IE of the organic semiconductor. The Ohmic-contact formation is illustrated for a number of material combinations and solves the problem of hole injection into organic semiconductors with a high IE of up to 6 eV.

One of the most important requirements for efficient organic-semiconductor devices is the establishment of Ohmic contacts for holes and electrons. To create an Ohmic contact for holes, the electrode work function should match the ionization energy (IE) of the organic semiconductor. In organic light-emitting diodes (OLEDs), materials with an IE as high as 6 eV are commonly used as hosts and emitters[1,2]. However, typical electrodes used in organic devices, such as indium-tin oxide (ITO) and poly(3,4-ethylenedioxythiophene)-poly(styrenesulfonate) (PEDOT:PSS) have work functions close to 5.0 eV (refs [3,4]), which give rise to large injection barriers. Since the injected current depends exponentially on the injection barrier[5], it is vital to find hole-injecting electrodes with a considerably higher work function. For example, chlorinated ITO can reach work functions of up to 6.1 eV (ref. [4]). However, a sizable contact barrier of about 0.5 eV was still observed when the electrode was put in contact with the popular 4,4′-bis(N-carbazolyl)biphenyl (CBP) organic host material, which has an IE of 6.0 eV (ref. [4]).

An alternative method to obtain Ohmic contacts is the use of a p-type doped hole-injection layer. The resulting strong band bending in the doped layer then allows for injection via tunnelling. However, a typical p-type dopant such as F6TCNNQ has an electron affinity of ~5.6 eV (ref. [6]), such that doping will not be effective for semiconductors with an IE larger than 5.6 eV. Very recently, a strategy was reported to achieve doped organic-semiconductor films with work functions up to 5.8 eV (ref. [7]). Using a doped polymer film as a hole-injection layer, it was shown that hole injection into a conjugated polymer with an IE of 5.8 eV was almost as efficient as the injection from a thermally evaporated MoO_3 reference.

MoO_3 is widely used as a hole contact in organic solar cells and OLEDs, owing to its extremely high work function of 6.9 eV (ref. [8]). MoO_3 is an n-type semiconductor, with an electron affinity of 6.7 eV and an ionization energy of 9.7 eV (ref. [8]). Because of its high electron affinity, MoO_3 can be used as a p-type dopant in CBP (ref. [9]). Since transition-metal oxides like MoO_3, V_2O_5 and WO_3 possess the combined quality of optical transparency and a very high work function of 6.7–7.0 eV, they seem to be ideal hole contacts, and are frequently applied in organic-semiconductor devices[10].

Here, we demonstrate that despite their high work function, transition-metal oxides give rise to a considerable injection barrier when put into contact with organic semiconductors. We present a strategy to completely eliminate this injection barrier by electrostatically decoupling the electrode from the organic semiconductor, enabling the formation of an Ohmic contact with organic semiconductors with an IE as high as 6 eV.

A direct way to investigate the hole-injection capability of an electrode into an organic semiconductor is to fabricate so-called hole-only devices. In such a device, an organic-semiconductor layer is sandwiched between two high-work-function electrodes, to prevent the injection of electrons. When applying a voltage across the device, the measured current is carried exclusively by holes, and the magnitude of the current is a measure of the hole-injection capabilities of one of the two electrodes, depending on the sign of the applied voltage. Since the current depends exponentially on the injection barrier[5], the measured current is very sensitive to changes in the barrier height. When the barrier height approaches zero, the contact can be regarded as Ohmic, and a transition from an injection-limited current into a space-charge-limited current will occur, which is governed by the charge-carrier mobility of the organic semiconductor[11,12].

In Fig. 1a, the current through a hole-only device of the organic semiconductor 2,2′,7,7′-tetrakis(*N*,*N*-diphenylamino)-9,9-spirobifluorene (Spiro-TAD) is displayed. Here, Spiro-TAD is sandwiched between a PEDOT:PSS bottom electrode and a MoO_3(10 nm)/Al top electrode. Since Spiro-TAD has a moderate IE of 5.3 eV (ref. [13]), hole injection from MoO_3 with a high work function of 6.9 eV is expected to be efficient. Surprisingly, as can be seen in Fig. 1, the current injected from MoO_3 (forward bias) is even lower than the current injected from PEDOT:PSS (reverse bias). Apparently,

[1]Max Planck Institute for Polymer Research, Mainz, Germany. [2]The Institute of Scientific and Industrial Research (ISIR), Osaka University, Ibaraki, Japan. *e-mail: wetzelaer@mpip-mainz.mpg.de

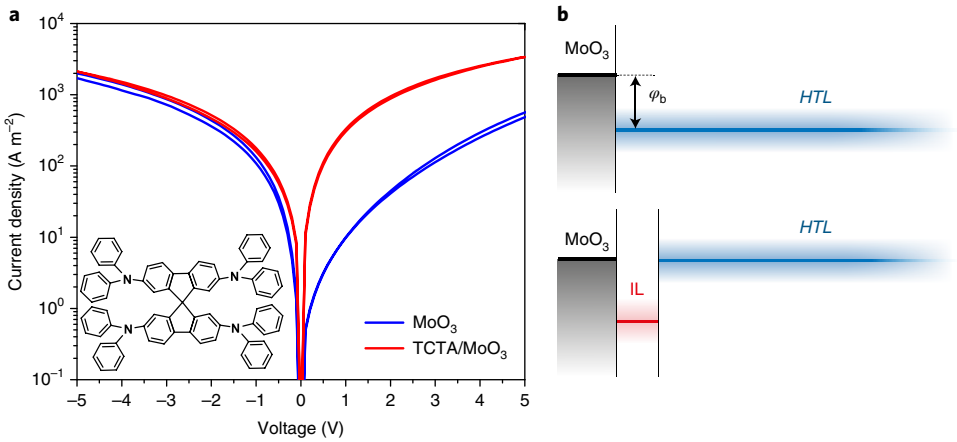

Fig. 1 | Hole-injection enhancement in Spiro-TAD. a, Current density–voltage characteristics of a PEDOT:PSS/Spiro-TAD/MoO_3 hole-only device with and without a TCTA (5 nm) interlayer between the Spiro-TAD (163 nm) transport layer and MoO_3. Negative bias corresponds to hole injection from the PEDOT:PSS, positive bias to hole injection from MoO_3. The inset shows the molecular structure of Spiro-TAD. **b**, Schematic energy-band diagram showing the effective injection barrier (φ_b) between MoO_3 and the hole-transport layer (HTL). Introducing an interlayer (IL) with a higher IE realigns the Fermi level with the IE of the HTL.

a hole-injection barrier at the Spiro-TAD/MoO_3 interface is present that lowers the injected current. As also can be observed in Fig. 1a, the hole injection is improved considerably by inserting a 5 nm layer of tris(4-carbazoyl-9-ylphenyl)amine (TCTA) between Spiro-TAD and MoO_3. By using the TCTA interlayer, the current injected from MoO_3 increases by over an order of magnitude, up to a factor of 30. This is a counterintuitive result, since TCTA has a higher IE (5.7 eV; ref. [14]) than Spiro-TAD, which usually aggravates hole-injection problems.

To demonstrate that the injection barrier at the organic/MoO_3 interface is not an exclusive property of Spiro-TAD, Fig. 2 shows that a similar hole-injection barrier exists between MoO_3 and the organic small molecules TCTA and CBP, which have IE values of 5.7 eV and 6.0 eV, respectively[14]. For both materials, the current injected from MoO_3 is improved by more than an order of magnitude by inserting a 5 nm interlayer of an organic semiconductor with a higher IE. In fact, independent of the material used for the interlayer, the current is universally improved to the same magnitude and voltage dependence, even for a material with a high IE, such as CBP.

Identical improvements were obtained for the high-work-function metal oxides WO_3 and V_2O_5, as shown in the Supplementary Information. It is also demonstrated in the Supplementary Information that equally high currents are obtained when applying the interlayer strategy to the bottom electrode. MoO_3 can diffuse into the organic layers when it is deposited on top of organic semiconductors, while a non-intermixed interface is obtained when organic layers are deposited on top of MoO_3 (ref. [14]). Despite deposition-order inversion, improvements in hole injection are identical, ruling out diffusion of MoO_3 as the mechanism for the observed hole-injection enhancement.

Figure 2b also shows how problematic hole injection into CBP is with conventional hole-injection layers such as PEDOT:PSS (reverse bias). The current in reverse bias is around five orders of magnitude lower than the current injected in forward bias, which is the result of the hole-injection barrier arising from the mismatch between the work function of PEDOT:PSS (5.0–5.2 eV) and the IE of CBP.

From the results on Spiro-TAD (see Supplementary Information), TCTA and CBP, it is inferred that hole injection is improved universally when the offset between the IE of the interlayer and trans-

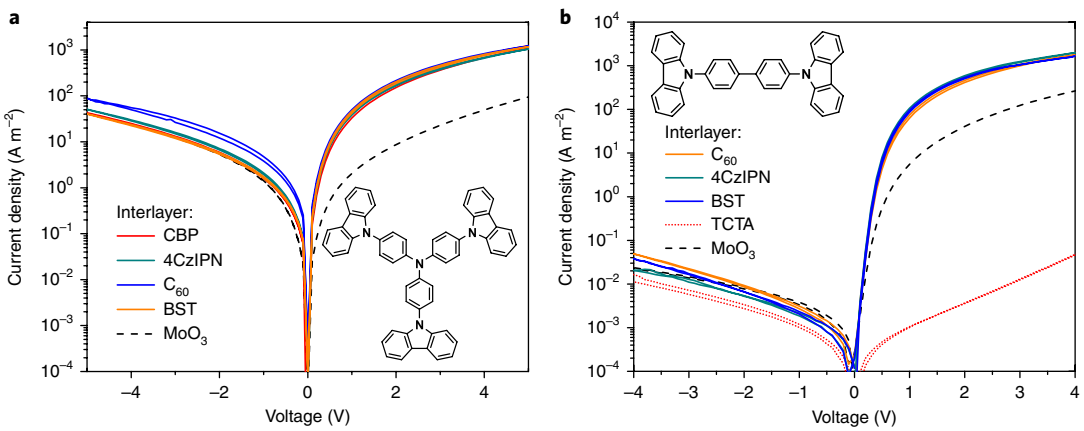

Fig. 2 | Hole-injection enhancement with different interlayers. a,**b**, Current density–voltage characteristics of TCTA (**a**; 239 nm) and CBP (**b**; 215 nm) hole-only devices with different interlayers. The hole current injected from MoO_3 (positive bias) improves to the same level whenever the IE of the interlayer is larger than the IE of the transport layer. For the case of CBP with a TCTA interlayer (**b**; red dotted line), the offset in IE is negative, resulting in a large reduction of the injected current. The insets in **a** and **b** show the molecular structures of TCTA and CBP, respectively.

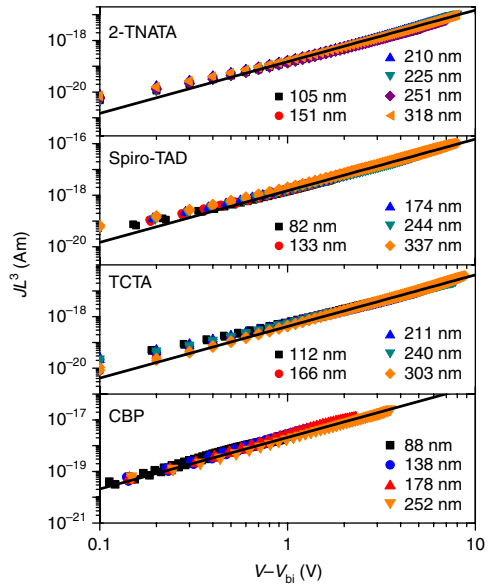

Fig. 3 | Space-charge-limited hole currents in four different materials. TCTA was used as an interlayer for 4,4′,4′′-tris[2-naphthyl(phenyl)amino] triphenylamine (2-TNATA) and Spiro-TAD transport layers, whereas CBP and BST interlayers were used for TCTA and CBP transport layers, respectively. For all materials, JL^3 is plotted for a range of layer thicknesses against voltage, corrected for the built-in voltage and the electrode series resistance. The lines represent fits with equation (1), from which the hole mobility is extracted.

port material is larger than 0.2–0.3 eV. Conversely, when the IE of the interlayer is lower than the IE of the transport material, resulting in an energetic staircase, the injected current drops by several orders of magnitude. This is demonstrated in Fig. 2b for the case of a TCTA interlayer on CBP, for which the IE offset has a negative value of −0.3 eV. It appears that there is no maximum to the value of the offset: the improvement in injection is observed for offsets of more than 1 eV.

The fact that the current for all investigated organic semiconductors reaches a maximum magnitude independent of the interlayer used strongly suggests that the current is no longer injection limited. This would imply that the use of an interlayer results in the formation of an Ohmic contact. To validate this hypothesis, it should be verified that the injected currents are space-charge limited. A space-charge-limited current is the maximum electrostatically allowed current that can pass through the organic-semiconductor layer. A trap-free space-charge-limited current is characterized by the Mott–Gurney square law[15]

$$J=\frac{9}{8}\varepsilon\mu\frac{(V-V_{bi})^2}{L^3} \quad (1)$$

where J is the current density, ε is the permittivity, μ is the charge-carrier mobility, V is the applied voltage, V_{bi} is the built-in voltage due to asymmetric work functions of the electrodes, and L is the layer thickness.

To test if the injected hole currents are indeed space-charge limited, the current needs to fulfill two important criteria: the current depends quadratically on voltage; and the current scales inversely with layer thickness to the third power. The layer-thickness dependence can be directly confirmed by plotting JL^3 against voltage. In case of a space-charge-limited current, the measured current for a range of layer thicknesses will collapse onto a single curve. This is indeed the case, as shown in Fig. 3. For all tested organic semiconductors, the L^{-3} layer-thickness dependence is fulfilled. In addition, the experimental current depends on the square of voltage, proving that the injected current is indeed space-charge limited. The establishment of a space-charge-limited current after insertion of the interlayer confirms the formation of an Ohmic hole contact. These results therefore demonstrate the formation of a truly Ohmic contact on organic semiconductors with an IE of up to 6 eV.

A space-charge-limited current can also be used to determine the charge-carrier mobility of organic semiconductors, as is evident from equation (1). The mobilities determined for 2-TNATA, Spiro-TAD, TCTA and CBP are in excellent agreement with the low-field values measured by the time-of-flight technique (see Table 1). It is known that the time-of-flight technique can overestimate the mobility, especially when charge trapping is present[16]. However, the fact the mobilities from space-charge-limited currents are close to the time-of-flight values shows that hole injection is indeed maximized (Ohmic contact) by using an interlayer and also that the current is not decreased by trapping effects. Interestingly, as a result of the high injection efficiency of the interlayer-enhanced contact, the space-charge conductivity of an 88 nm undoped CBP layer amounts to 2.5×10^{-6} S cm^{-1}, which even surpasses the conductivity of highly p-doped CBP with 22.1 mol% of MoO_3 (1×10^{-6} S cm^{-1})[9].

Knowing the hole mobilities from the measured space-charge-limited currents, we can now determine the injection barriers from the injection-limited currents observed for transition-metal oxide electrodes (MoO_3, V_2O_5 and WO_3) without an interlayer. For all investigated organic semiconductors and metal oxides, an injection barrier of 0.39 ± 0.03 eV was determined (see Supplementary Information), independent of the IE of the organic semiconductor. Interestingly, a universal energy-alignment behaviour between metal oxides and organic semiconductors has been reported, where a general 0.3 eV offset was observed between the work function of the oxide and the IE of the organic semiconductor[17]. These ultraviolet photoelectron spectroscopy (UPS) measurements suggest that the energy offset is manifested as an injection barrier.

To unravel the mechanism of the Ohmic-contact formation, the energy-level alignment in the presence of an interlayer was investigated. For this purpose, UPS measurements were performed layer-by-layer on a representative MoO_3/TCTA/2-TNATA structure, which has an IE offset of 0.7 eV between the TCTA interlayer and 2-TNATA. Figure 4a shows the measured IE as a function of layer thickness. At a TCTA coverage of 1 nm, the Fermi level of MoO_3 is pinned at 0.38 eV below the IE of TCTA, in line with the universal offset in the pinning regime[17]. With increasing TCTA thickness, the IE separates further from the Fermi level to 0.6 eV at 5 nm, which

Table 1 | Ionization energies and hole mobilities of materials used in this work

Material	IE (eV)	SCLC mobility ($m^2V^{-1}s^{-1}$)	TOF mobility ($m^2V^{-1}s^{-1}$)
2-TNATA	5.0 (ref. [17])	5×10^{-9}	3×10^{-9} (ref. [25])
Spiro-TAD	5.3 (ref. [13])	5×10^{-8}	3×10^{-8} (ref. [26])
TCTA	5.7 (ref. [14])	1.4×10^{-8}	2×10^{-8} (ref. [27])
CBP	6.0 (refs [14,17])	7×10^{-8}	5×10^{-8} (ref. [28])
4CzIPN	6.1 (ref. [23])	-	-
C_{60}	6.4 (ref. [14])	-	-
BST	7.0 (this work)	-	-

IEs are obtained with ultraviolet photoelectron spectroscopy. Mobilities are obtained from space-charge-limited currents (Fig. 3), which are compared to time-of-flight measurements from the literature.

abruptly reduces to 0.16 eV upon 2-TNATA coverage, because of the IE offset between TCTA (5.7 eV) and 2-TNATA (5.0 eV). This shows that, near the interface, the IE of 2-TNATA aligns with the Fermi level, which is the required condition for the formation of an Ohmic contact. The energy offset of 0.16 eV is substantially smaller than the universal offset of 0.3 eV in the monolayer regime as previously observed[17], explaining the improved injection with the help of the interlayer.

To understand the band alignment as well as the (universal) barrier reduction, the IE profile was calculated by solving Poisson's equation, as described in the Supplementary Information. The Poisson equation relates charge density to electrostatic potential, both of which depend on the relative alignment of the oxide Fermi level with respect to the density of states (DOS) of the organic semiconductor[18–20]. As shown in Fig. 4a, within the first nanometre, a strong band bending is observed as a result of charge transfer between MoO_3 and TCTA to establish thermodynamic equilibrium across the interface. In the monolayer regime, the Fermi level is (universally[14,17]) pinned at 0.3–0.4 eV below the IE of TCTA, which could be reproduced by considering a broadened DOS near the metal oxide, as suggested in previous publications[19,21,22]. Effectively, the Fermi level is pinned to the deeper states in the broadened interface DOS, from which charges have to escape to the narrower bulk DOS, leading to an injection barrier. The band bending for increasing layer thickness is described well by including a Coulomb image potential due to differences in dielectric constants between MoO_3 and the organic semiconductor (see Supplementary Information). We suggest DOS broadening at the interface and the attractive image potential to be the reason for the observed injection barriers at the metal-oxide contact.

At the TCTA/2-TNATA interface, the calculations support alignment of the IE of 2-TNATA with the Fermi level, which is accompanied by the presence of a high hole density (inset Fig. 4). The experimental IE profile of the 2-TNATA layer is consistently described by using a Gaussian DOS width of 0.1 eV, without additional broadening. This disorder value is also consistent with molecular dynamics simulations of layered structures and evaluated energetic disorder in the organic films using polarizable force fields, showing no distinct DOS broadening at the organic/organic interfaces, as described in the Supplementary Information. In short, the interlayer realigns the Fermi level with the IE of the organic semiconductor, negating the barrier formation due to DOS broadening and the image potential by effectively decoupling the electrode and semiconductor electrostatically.

With the developed model, we can now explore the limiting cases for the formation of an Ohmic contact by simulating band diagrams. By varying the interlayer IE in Fig. 4b, it is found that the IE in the HTL is close to the Fermi level for an interlayer offset of at least ~0.3 eV, with larger offsets having no effect on the energetic position of the HTL, as confirmed experimentally in Fig. 2 by the identical currents obtained for different interlayers with varying offsets. In a similar fashion, electrode work functions that are equal to or higher than the IE of the HTL are required (Fig. 4c), which is the case in our injection experiments with the high-work-function metal oxides MoO_3, V_2O_5 and WO_3.

The UPS measurements and simulations indicate a high hole density at the organic/organic interface [inset Fig. 4a), which plays the role of a virtual Ohmic hole contact, spatially separated from the electrode by the interlayer. However, charges still have to pass through the interlayer to contribute to the current. Considering the measured space-charge-limited currents with mobilities that are close to the time-of-flight values, even for thin transport layers of less than 100 nm, it can be concluded that the interlayer does not add a significant resistance. In addition, as can be seen from the experimental currents in reverse bias, where the current is injected from the PEDOT:PSS electrode, the presence of the interlayer does not reduce the current, even for large IE offsets between the transport material and the interlayer, which normally imposes a hole-extraction barrier. This indicates that the interlayer is virtually transparent for holes.

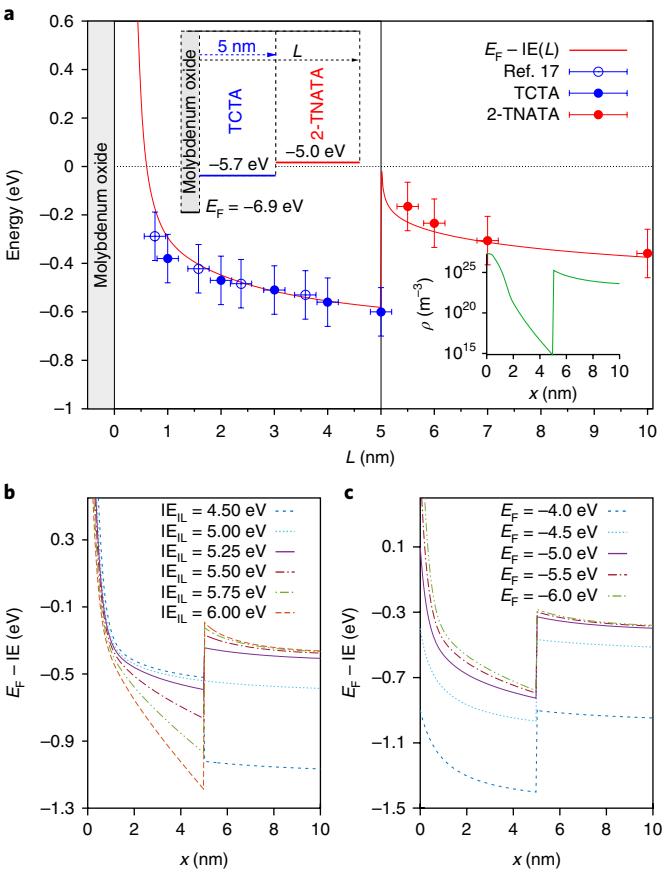

Fig. 4 | Experimental and calculated IE profiles across interlayer/hole-transport layer structures. a, IE onset with respect to the Fermi level obtained by UPS layer by layer across a MoO_3/TCTA(5 nm)/2-TNATA(5 nm) structure (filled symbols), augmented with data of the universal IE profile of organic semiconductors on metal oxides[17] (open symbols). The error bars indicate an estimated error of ±0.1 eV for the IE and ±0.2 nm for the layer thickness. The calculated IE position at the layer surface (red line), corresponding to the UPS measurements, is obtained by evaluating the band bending at $x = L$ for different L. The top inset shows the energy levels of the separate materials and the bottom inset shows the calculated charge density across the layers. **b**, Simulated band diagrams (IE as a function of position x across the layers) for different interlayer IEs, using a work function of 6.9 eV and a HTL IE of 5.0 eV. **c**, Band diagrams for different work functions, with an IE of 5.5 eV for the interlayer and 5.0 eV for the HTL.

Since the measured current is the same regardless of the interlayer material, it appears that the transport properties of different interlayers do not affect the injected current. However, at interlayer thicknesses above 5 nm, the current is reduced and depends on the interlayer material (see Supplementary Information), suggesting that transport through and injection into the interlayer becomes a limiting factor. This supports a scenario in which charges tunnel through the electrostatic barrier of the interlayer to the second layer. For thick interlayers, the charge density decreases and the tunnelling rates become negligible, thus explaining that the optimal interlayer thickness is below 5 nm. On the other hand, the optimum thickness of 3–5 nm helps to decrease the barrier due to the attractive image potential near the electrode interface, which is strongly reduced at these length scales.

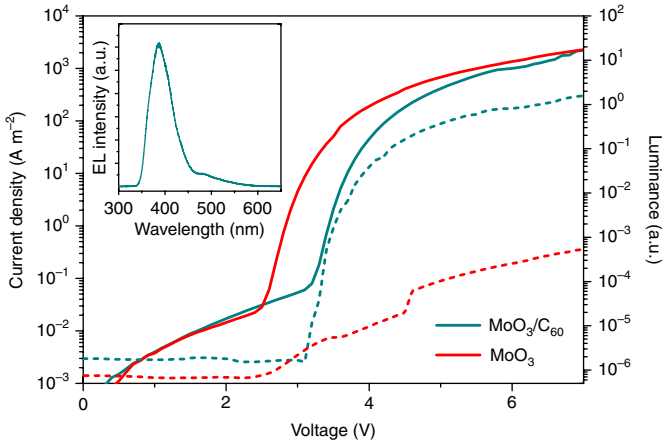

Fig. 5 | UV-emitting TPBi OLEDs. Current density–voltage (solid lines) and luminance–voltage (dashed lines) characteristics of OLEDs with a MoO_3/[C_{60}(4 nm)]/TPBi(58 nm)/Ba/Al structure, with and without a C_{60} interlayer. The inset shows the electroluminescence spectrum corresponding to TPBi emission, with an onset at 340 nm and a maximum at 385 nm.

As an ultimate proof, we demonstrate our hole injection strategy in a light-emitting diode based on the electron-transport material 1,3,5-tris(*N*-phenylbenzimidazol-2-yl)benzene (TPBi). Because of its high ionization energy of 6.3 eV, TPBi is frequently used as a hole-blocking material in OLEDs[23,24]. Here, we use TPBi in an ultraviolet-emitting diode, consisting of TPBi sandwiched between a MoO_3 anode and a Ba cathode. As demonstrated in Fig. 5, adding an additional C_{60} interlayer between MoO_3 and TPBi results in a three orders of magnitude increased light output and efficiency. The increased light output is a direct consequence of the enhanced hole injection, showing that it is possible to directly inject holes even in materials that are normally used for hole-blocking purposes. Since TPBi is an electron transporter[24], the current through the OLED is mainly carried by electrons and does not increase by improving the hole contact. However, the *J*–*V* characteristics are shifted by 0.6 V along the voltage axis, which is the result of an increased built-in voltage due to the reduced barrier on the anode side, which in turn enhances the hole injection and light output.

In conclusion, we present a universal strategy for achieving Ohmic hole contacts on organic semiconductors with a high IE. In particular, the injected hole current is consistently improved by over an order of magnitude as compared to high-work-function transition-metal oxide electrodes. The barrier reduction is rationalized by electrostatic decoupling of the electrode from the organic semiconductor with an interlayer. This interlayer strongly reduces the effect of the attractive image potential near the electrode interface, and eliminates the DOS broadening present at the organic/electrode interface, while restoring Fermi-level alignment. As a proof of principle, we illustrate that the interlayer-enhanced contact can be used in an ultraviolet-emitting diode, providing direct hole injection into the hole-blocking material TPBi. The presented efficient hole injection into organic semiconductors with ionization energies beyond 6 eV extends the range of materials available for OLEDs and organic photovoltaic devices, which otherwise would suffer from high contact barriers.

Methods

Methods, including statements of data availability and any associated accession codes and references, are available at https://doi.org/10.1038/s41563-018-0022-8.

Received: 21 September 2017; Accepted: 15 January 2018;
Published online: 19 February 2018

References

1. Tao, Y., Yang, C. & Qin, J. Organic host materials for phosphorescent organic light-emitting diodes. *Chem. Soc. Rev.* **40**, 2943–2970 (2011).
2. Wong, M. Y. & Zysman-Colman, E. Purely organic thermally activated delayed fluorescence materials for organic light-emitting diodes. *Adv. Mater.* **29**, 1605444 (2017).
3. Koch, N. & Vollmer, A. Electrode-molecular semiconductor contacts: Work-function-dependent hole injection barriers versus Fermi-level pinning. *Appl. Phys. Lett.* **89**, 162107 (2006).
4. Helander, M. G. et al. Chlorinated indium tin oxide electrodes with high work function for organic device compatibility. *Science* **332**, 944–947 (2011).
5. Simmons, J. G. Richardson–Schottky effect in solids. *Phys. Rev. Lett.* **15**, 967–968 (1965).
6. Méndez, H. et al. Charge-transfer crystallites as molecular electrical dopants. *Nat. Commun.* **6**, 8560 (2015).
7. Tang, C. G. et al. Doped polymer semiconductors with ultrahigh and ultralow work functions for ohmic contacts. *Nature* **539**, 536–540 (2016).
8. Kröger, M. et al. Role of the deep-lying electronic states of MoO_3 in the enhancement of hole-injection in organic thin films. *Appl. Phys. Lett.* **95**, 123301 (2009).
9. Kröger, M. et al. P-type doping of organic wide band gap materials by transition metal oxides: A case-study on molybdenum trioxide. *Org. Electron.* **10**, 932–938 (2009).
10. Meyer, J. et al. Transition metal oxides for organic electronics: Energetics, device physics and applications. *Adv. Mater.* **24**, 5408–5427 (2012).
11. Blom, P. W. M., de Jong, M. J. M. & Vleggaar, J. J. M. Electron and hole transport in poly(p-phenylene vinylene) devices. *Appl. Phys. Lett.* **68**, 3308–3310 (1996).
12. Davids, P. S., Campbell, I. H. & Smith, D. L. Device model for single carrier organic diodes. *J. Appl. Phys.* **82**, 6319–6325 (1997).
13. Belisle, R. A., Jain, P., Prasanna, R., Leijtens, T. & McGehee, M. D. Minimal effect of the hole-transport material ionization potential on the open-circuit voltage of perovskite solar cells. *ACS Energy Lett.* **1**, 556–560 (2016).
14. White, R. T., Thibau, E. S. & Lu, Z.-H. Interface structure of MoO_3 on organic semiconductors. *Sci. Rep.* **6**, 21109 (2016).
15. Mott, N. F. & Gurney, R. W. *Electronic Processes in Ionic Crystals* (Oxford University Press: Oxford, 1940).
16. Li, C., Duan, L., Li, H. & Qiu, Y. Universal trap effect in carrier transport of disordered organic semiconductors: Transition from shallow trapping to deep trapping. *J. Phys. Chem. C* **118**, 10651–10660 (2014).
17. Greiner, M. T. et al. Universal energy-level alignment of molecules on metal oxides. *Nat. Mater.* **11**, 76–81 (2012).
18. Blakesley, J. C. & Greenham, N. C. Charge transfer at polymer-electrode interfaces: The effect of energetic disorder and thermal injection on band bending and open-circuit voltage. *J. Appl. Phys.* **106**, 034507 (2009).
19. Oehzelt, M., Koch, N. & Heimel, G. Organic semiconductor density of states controls the energy level alignment at electrode interfaces. *Nat. Comm.* **5**, 4174 (2014).
20. Oehzelt, M., Akaike, K., Koch, N. & Heimel, G. Energy-level alignment at organic heterointerfaces. *Sci. Adv.* **1**, e1501127 (2015).
21. Baldo, M. A. & Forrest, S. R. Interface-limited injection in amorphous organic semiconductors. *Phys. Rev. B* **64**, 085201 (2001).
22. Limketkai, B. N. & Baldo, M. A. Charge injection into cathode-doped amorphous organic semiconductors. *Phys. Rev. B* **71**, 085207 (2005).
23. Seino, Y., Inomata, S., Sasabe, H., Pu, Y.-J. & Kido, J. High-performance green OLEDs using thermally activated delayed fluorescence with a power efficiency of over 100 lm W^{-1}. *Adv. Mater.* **28**, 2638–2643 (2016).
24. Hung, W.-Y. et al. Employing ambipolar oligofluorene as the charge-generation layer in time-of-flight mobility measurements of organic thin films. *Appl. Phys. Lett.* **88**, 064102 (2006).
25. Tse, S. C., Kwok, K. C. & So, S. K. Electron transport in naphthylamine-based organic compounds. *Appl. Phys. Lett.* **89**, 262102 (2006).
26. Bach, U., De Cloedt, K., Spreitzer, H. & Grätzel, M. Characterization of hole transport in a new class of spiro-linked oligotriphenylamine compounds. *Adv. Mater.* **12**, 1060–1063 (2000).
27. Noh, S., Suman, C. K., Hong, Y. & Lee, C. Carrier conduction mechanism for phosphorescent material doped organic semiconductor. *J. Appl. Phys.* **105**, 033709 (2009).
28. Matsusue, N., Suzuki, Y. & Naito, H. Charge carrier transport in neat thin films of phosphorescent iridium complexes. *Jpn. J. Appl. Phys.* **44**, 3691–3694 (2005).

Acknowledgements

The authors thank C. Bauer, F. Keller, and H.-J. Guttmann for technical support. This project has received funding from the European Union Horizon 2020 research

and innovation programme under Grant Agreement No. 646176 (EXTMOS). D.A. thanks the BMBF grant InterPhase (FKZ 13N13661) and the European Union Horizon 2020 research and innovation programme 'Widening materials models' under Grant Agreement No. 646259 (MOSTOPHOS).

Author contributions

G.A.H.W. proposed and supervised the project. N.B.K. carried out sample preparation and electrical measurements. H.L. performed the UPS measurements. D.A. and A.M. performed molecular-dynamics and energy-alignment simulations. Y.I. synthesized and purified 4CzIPN. G.A.H.W., N.B.K. and P.W.M.B. analysed the experimental data. G.A.H.W. wrote the manuscript with input from D.A. and P.W.M.B.

Competing interests

The authors declare no competing financial interests.

Additional information

Supplementary information is available for this paper at https://doi.org/10.1038/s41563-018-0022-8.

Reprints and permissions information is available at www.nature.com/reprints.

Correspondence and requests for materials should be addressed to G.-J.A.H.W.

Publisher's note: Springer Nature remains neutral with regard to jurisdictional claims in published maps and institutional affiliations.

Methods

Materials. 1,2,3,5-tetrakis(carbazol-9-yl)-4,6-dicyanobenzene (4CzIPN) was synthesized according to the procedure described in the literature[29] and purified by vacuum sublimation. 4,4′′-bis(triphenylsilanyl)-(1,1′,4′,1′′)-terphenyl (BST) was purchased from Luminescence Technology Corp. and all other materials were purchased from Sigma-Aldrich and used as received.

Device fabrication and measurement. Hole-only devices were fabricated in a glass/ITO/PEDOT:PSS(35 nm)/hole-transport layer/[interlayer]/metal oxide(10 nm)/Al(100 nm) structure, in which the metal oxide was either MoO_3, WO_3, or V_2O_5. PEDOT:PSS was deposited by spin coating, and subsequent layers were thermally evaporated at a base pressures of $4–5\times10^{-7}$ mbar. Symmetric devices were prepared in a glass/ITO/PEDOT:PSS/metal oxide/interlayer/hole-transport layer/interlayer/metal oxide/Al structure. OLEDs were fabricated in a glass/ITO/PEDOT:PSS/MoO_3/[C_{60}(4 nm)]/TPBi(58 nm)/Ba(5 nm)/Al(100 nm) structure. Electrical characterization was carried out under N_2 atmosphere with a Keithley 2400 source meter, light output was recorded with a calibrated Si photodiode, and electroluminescence spectra were obtained with a USB4000-UV-VIS-ES spectrometer.

UPS characterization. UPS measurements were conducted at a base pressure of 10^{-9} mbar on Si/Cr(2 nm)/Au(50 nm)/MoO_3(10 nm)/organic substrates with a Kratos Axis Ultra^{DLD} spectrometer (Kratos, Manchester, UK). During UPS measurement, the sample was held at a bias of −9 V with respect to the spectrometer. Illumination at 21.22 eV was provided by the He(I) emission line from a helium discharge lamp. Photoelectron emission was collected at 0° from the surface normal of the samples. The spectra were taken in three different spots to confirm their reproducibility and the irradiation exposure time was kept under one minute.

Molecular simulations and density of states evaluation. All morphology simulations were performed using the GROMACS package and re-parametrized OPLS-AA force-field, as described in the Supplementary Information. Density of states was evaluated using the VOTCA package[30,31] and polarizable force-field (Thole model) as described in the Supplementary Information.

Data availability. Experimental data are available from the corresponding author upon reasonable request.

References

29. Uoyama, H., Goushi, K., Shizu, K., Nomura, H. & Adachi, C. Highly efficient organic light-emitting diodes from delayed fluorescence. *Nature* **492**, 234–238 (2012).
30. Ruehle, V. et al. Microscopic simulations of charge transport in disordered organic semiconductors. *J. Chem. Theory Comput.* **7**, 3335–3345 (2011).
31. Poelking, C. & Andrienko, D. Long-range embedding of molecular ions and excitations in a polarizable molecular environment. *J. Chem. Theory Comput.* **12**, 4516–4523 (2016).